JET–P(98)33

K D Lawson et al

An Empirical Method for the Determination of Elemental Components of Radiated Powers and Impurity Concentrations from VUV and XUV Spectral Features in Tokamak Plasmas

JET–P(98)33

An Empirical Method for the Determination of Elemental Components of Radiated Powers and Impurity Concentrations from VUV and XUV Spectral Features in Tokamak Plasmas

K D Lawson[1], N J Peacock[1], R Giannella[2], N A C Gottardi[3], N C Hawkes[1], L Lauro-Taroni, P D Morgan, M G O'Mullane[4], T K Patel[5], P Smeulders.

JET Joint Undertaking, Abingdon, Oxfordshire, OX14 3EA,
[1]Euratom/UKAEA Fusion Association, Culham Science Centre, Abingdon, Oxon, OX14 3DB.
[2]Association Euratom–CEA, CE Cadarache, 13108, Saint Paul lez Durance, France.
[3]Commission European Community, DGXVII, E2 Batiment Cube, L 2920, Luxembourg.
[4]Dept. of Physics and Applied Physics, University of Strathclyde, 107 Rotten Row, Glasgow, G4 0NG.
[5]MCAT Inc.,, NASA Ames Research Centre, MS 258-1, Moffett Field, CA 94035-1000, USA

Preprint of a Paper submitted for publication in Physics Scripta

December 1998

ABSTRACT

The derivation of elemental components of radiated powers and impurity concentrations in bulk tokamak plasmas is complex, often requiring a full description of the impurity transport. A novel, empirical method, the Line Intensity Normalization Technique (LINT) has been developed on the JET (Joint European Torus) tokamak to provide routine information about the impurity content of the plasma and elemental components of radiated power (P_{rad}). The technique employs a few VUV and XUV resonance line intensities to represent the intrinsic impurity elements in the plasma. From a data base comprising these spectral features, the total bolometric measurement of the radiated power and the Z_{eff} measured by visible spectroscopy, separate elemental components of P_{rad} and Z_{eff} are derived. The method, which converts local spectroscopic signals into global plasma parameters, has the advantage of simplicity, allowing large numbers of pulses to be processed, and, in many operational modes of JET, is found to be both reliable and accurate. It relies on normalizing the line intensities to the absolute calibration of the bolometers and visible spectrometers, using coefficients independent of density and temperature. Accuracies of the order of ±15% can be achieved for the elemental P_{rad} components of the most significant impurities and the impurity concentrations can be determined to within ±30%. Trace elements can be monitored, although with reduced accuracy. The present paper deals with limiter discharges, which have been the main application to date.

As a check on the technique and to demonstrate the value of the LINT results, they have been applied to the transport modelling of intrinsic impurities carried out with the SANCO transport code, which uses atomic data from ADAS. The simulations provide independent confirmation of the concentrations empirically derived using the LINT technique. For this analysis, the simple case of the L-mode regime is considered, the chosen pulses having two significant impurity elements. The data for the low Z element, C, suggest the need for an edge transport barrier. The modelling of the higher Z element, Ni, allows the bulk transport parameters to be determined. The balance of the plasma particle inventory leads to a linear relationship between the outer diffusion coefficient and the edge transport barrier. In contrast to the results reported previously by Giannella *et al*. (1994), no significant convection term is required inside this edge barrier.

1. INTRODUCTION

For the efficient operation of large plasma machines, routine information on the impurity content of the plasma is an important diagnostic requirement. Depending on the application, the impurity data are most usefully provided either as concentrations or as total powers radiated by each impurity element (P_{rad}). Ideally, these data are derived during plasma operations as part of an intershot or real time analysis. They are also of value in subsequent more detailed analyses of particular physics experiments. Two applications demonstrate the importance of both data sets. In high performance operational modes where the fuel ion dilution is of concern, such as can

occur when there is preferential impurity accumulation in the plasma core or in low density regimes like the 'hot ion' H-mode, knowledge of the impurity concentrations is vital. In other regimes, as for example in high density operation, it is the radiated power rather than the fuel dilution that largely determines the operational limits.

Both passive and active techniques are used routinely on JET to diagnose the impurity content. The present study involves the passive observation and spectral analysis of the VUV and XUV radiation emitted from the plasma. An example of an active technique is the interpretation of the emission due to atom-ion charge exchange collisions (von Hellermann and Summers 1993). An advantage of the analysis of the passive emission is its general use. In contrast, active techniques in JET can only be employed when additional heating neutral beams are injected, there being no neutral beams for diagnostic purposes per se.

The emission from intrinsic impurities depends on local plasma parameters such as the electron temperature, T_e, and density, n_e, and on the transport of impurity ions. Coronal ionization balance cannot be assumed throughout the plasma and so the analysis of the emission can only be treated using a full impurity transport simulation. Deviations from coronal balance are particularly severe towards the plasma edge, where the particle and temperature gradient terms in the transport equations are particularly important, and from where a significant proportion of the radiation usually originates.

Validation of the experimental data and the assessment of other uncertainties in the transport and atomic physics modelling make a detailed transport simulation a complex and lengthy procedure. Clearly, such an approach would be very limiting when dealing with the large number of pulses, typically several thousand, encountered during a period of JET operations. In order to deal with these data, a novel empirical method, the Line Intensity Normalization Technique (LINT), has been devised to determine both impurity concentrations and elemental components of radiated powers. The LINT method is based upon the hypothesis that a representative ion with a characteristic VUV or XUV spectral line can be chosen for each significant impurity element and that each of these spectral line intensities has a linear relation to the contribution of that element to the total radiated power and to the effective ion charge, the Z_{eff}. If this hypothesis is correct, these elemental components should sum to give the total radiated power or Z_{eff} as measured by bolometry and visible spectroscopy, respectively. The method has the important advantage that the analysis is straightforward, enabling large numbers of pulses to be processed. It has been developed and used extensively in the analysis of JET impurity data. There is particular confidence in the derived elemental components of the radiated power.

Details of the spectrometers and the other instruments used to provide the experimental data are given in the next section and the LINT method is described in section 3. A number of examples are used to illustrate the technique's wide applicability, its present limitations being noted. When applying the technique, a marked difference is found between the limiter phase of a discharge and that with an X-point magnetic configuration. Not only does the more efficient

screening of the X-point phase reduce the impurity influx, but there appears to be a relative change in the electron density and temperature profiles at the plasma edge. The LINT method must therefore be applied to the two phases of the discharge separately. The limiter phase has been more widely studied and it is found that the relationship between the line intensities and the elemental components is more stable in this phase, this relationship being discussed in section 3.2. The present paper deals only with the application of the technique to limiter pulses.

Clearly, this empirical approach, which relates a characteristic spectral line measured along a single line of sight for each element to global parameters, is simplistic and needs extensive experimental verification. Some form of theoretical justification is also desirable. Experimentally, the justification for the LINT method rests in the consistency found between the empirical components and data obtained from the bolometers and measurements of the Z_{eff} derived from the visible bremsstrahlung for a sequence of pulses. The first pulses within the sequence are used to derive elemental P_{rad} components and concentrations, this analysis enabling predictions of these quantities to be made for subsequent pulses from the spectral information alone.

Although there is no complete theoretical understanding of the success of the LINT method, transport simulations of individual intrinsic impurities provide further and independent confirmation of the validity of the technique. The separation of the radiated power into elemental components and concentrations means that the LINT results are useful inputs to transport simulations of the individual impurities, providing additional constraints to the modelling. Such simulations give confirmation of the derived impurity concentrations. However, the complexity of the full transport modelling means that its precision is insufficient to validate the LINT radiated power components to their expected accuracy. In many pulses, the accuracy of the elemental P_{rad} components is higher when determined by the empirical method.

Simulations of L-mode limiter discharges, which demonstrate the value of the empirically derived data, are presented in section 4. In these pulses, there are just two significant impurity elements, one of medium atomic number (Z), Ni, and the other a low Z element, C. The presence of only two elements results in a high degree of confidence in the elemental radiated power components and concentrations determined by the LINT method. It is useful for one of the elements being studied to have a medium or high Z, since its different ionization stages will radiate line emission from a range of spatial locations throughout the plasma volume. This enables the local impurity transport parameters to be determined and a comparison is made between the simulation results and the available experimental data for the analysed pulses.

2. THE EXPERIMENTAL TECHNIQUES

2.1. Measurements used in the LINT method

The bolometric measurements on JET used in the present analyses were recorded by one vertical and two horizontal pinhole cameras situated at one toroidal location and eight single bolometers used to monitor the toroidal symmetry of the plasma emission (Mast *et al*. 1985). The vertical

pinhole camera contains 14 bolometers and the horizontal cameras each have 10, their lines of sight covering the whole of one poloidal cross-section. The bolometers use gold resistors and are sensitive both to particles and radiation in the wavelength range 1.5 to 2000Å. A check was made to see whether neutral particles might affect the measured powers. Assuming typical values for the neutral particle fluxes (Bracco *et al*. 1991), their contribution is not expected to be very significant (at most a few per cent) compared with that of the radiation in the limiter pulses being analysed. Particular consideration was given to the pulses to which the transport simulation (section 4) was applied; again the effect of the neutral particles is expected to be small. The vertical camera is used to derive the total radiated power, with an accuracy of better than ±10%.

The Z_{eff} is derived from the visible spectrum recorded with two channels, one having a vertical and the other a horizontal line of sight. The light is relayed from the JET machine by optical fibres to detectors outside the biological shield (Morgan *et al*. 1985). The continuum emission around a wavelength of 5235Å is observed with the use of a filter having a band-pass of 10Å FWHM. The line-integrated continuum emission along a line of length l is given by

$$\varepsilon_I \propto \int n_e^2(l)\, T_e^{-0.5}(l)\, Z_{eff}(l)\, dl,$$

from which, knowing the n_e and T_e profiles, a spatially averaged value of Z_{eff} can be calculated (Morgan and O'Rourke 1987). It is noted that, for the pulses modelled by the simulations described in section 4, only data from the vertical view were available.

The VUV spectrum of the bulk plasma in JET is monitored by a McPherson/Schoeffel SPRED instrument (Fonck *et al*. 1982), which employs a holographic, toroidal diffraction grating to give a flat focal field, while the XUV spectrum is recorded with a grazing incidence, SOXMOS instrument (Schwob *et al*. 1987). Both spectrometers have a near-horizontal line of sight close to the midplane of the torus. The SPRED instrument observes the spectrum at wavelengths longer than ~100Å, the observed spectral range and resolution depending on the diffraction grating employed. On JET, those most commonly used have a ruling density of either 450 or 2105g.mm^{-1}, the former giving a larger spectral coverage including wavelengths of up to ~1100Å and a resolution of ~4Å and the latter a higher resolution of ~1Å, but with a more limited spectral range of up to ~320Å. The SOXMOS spectrometer has two detectors, which can be moved independently along the Rowland circle to observe wavelengths from ~17Å up to ~340Å. Although each detector observes a comparatively narrow spectral range, the spectral resolution is significantly higher than that of the SPRED instrument. At short wavelengths, a range of about ~20Å is recorded with a spectral resolution of ~0.2Å, while at higher wavelengths the range increases to ~70Å with a resolution of ~0.4Å. An advantage of the LINT method is that no absolute sensitivity calibration is required for the spectrometers; such a calibration is difficult to achieve, particularly to the accuracy that can be readily obtained for the bolometers and visible spectrometers.

2.2 Additional measurements applied to the transport simulations

In the transport simulations, discussed in section 4, the VUV and XUV line intensities were compared directly with the modelled results. Such comparisons are particularly valuable when an absolute sensitivity calibration is available for the spectrometer. A calibration was obtained for the SPRED spectrometer from charge exchange measurements (Hawkes *et al*. 1992), additional data (Behringer 1987) leading to these results being modified. The final calibration used is given by Lawson *et al*. (1987). This instrument viewed the plasma via a gold-coated mirror, which had become degraded over a period of time and this led to uncertainty regarding the calibration for the shortest wavelengths. Comparing the ratios of the intensities of the NiXXVI doublet at 165 and 234Å and of the NiXVIII doublet at 292 and 321Å with the output of the transport simulations shows that there was no significant loss in mirror reflectivity for wavelengths above ~150Å. A comparison of transitions belonging to the same ionization stage minimizes the effect of the ion transport, the ratio depending largely on the atomic physics. Consequently, the sensitivity calibration given by Lawson *et al*. was used without modification for all lines except the 118Å, NiXXV line. The calibration at this wavelength was adjusted to match the simulations and it was found necessary to increase the inverse sensitivity by a factor of 5.3. The inverse sensitivity curve used is shown in figure 1. The accuracy of the absolute calibration is estimated to be better than ±40%. The time dependent line intensity is obtained by integrating the area under a particular spectral line for each time interval that the spectrum is recorded. The integration of the intensity of strong lines, well separated from their neighbours, can be performed to an accuracy of better than ±10%.

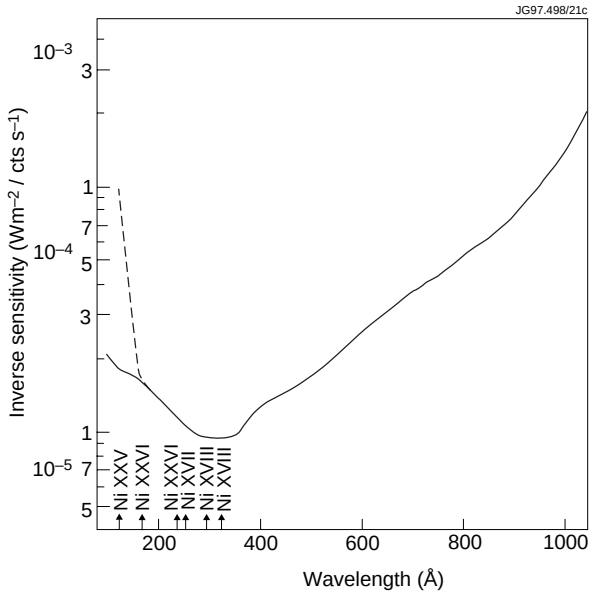

Figure 1. Inverse sensitivity calibration curve for the gold-coated mirror and SPRED spectrometer in the arrangement described by Fonck et al. *(1982) with a 450g.mm^{-1} grating and showing the change required to account for the damage to the mirror (-----). The wavelengths of the Ni spectral lines used in the transport analysis are indicated.*

No absolute sensitivity calibration is available for the XUV instrument. This did not affect the modelling of Ni, whose most intense spectrum falls in the VUV and soft X-ray regions. However, it did limit the usefulness of the simulations for C, the XUV region containing the CV and CVI resonance lines.

In the simulations, use has been made of a close positioning within the spectrum of certain Ni lines. This feature is useful since the relative sensitivity calibration for these emissions is known to a greater accuracy than the absolute calibration. The spectral region between ~150 and 350Å contains several Ni lines, whose positions are indicated in figure 1 and for which the relative error in calibration is

smaller than the absolute error, it being estimated to be less than ±20%. Of particular note is that the NiXXVI line at 234Å is adjacent in the spectrum to the NiXVII line at 249Å. As will be illustrated in section 4.3, the NiXXVI emission has a wide spatial extent centred at about half the minor radius of the plasma, whereas the NiXVII emission originates from a narrow shell near the plasma edge. The closeness of the wavelengths of these spectral lines is advantageous given the spatial separation of the emitting volumes. The relative error in their sensitivity calibration is expected to be smaller than ±10%, this putting a very stringent constraint on the simulations.

The other experimental measurement that has been directly compared with the results of the simulations is of the spectrally integrated soft X-ray emission. This is recorded by two, soft X-ray 'pinhole' cameras, which employ arrays of silicon diode detectors (Edwards *et al*. 1986). One of the cameras views the plasma horizontally with a fan of 62 lines of sight; the other, a vertical camera, has a fan of 38 viewing lines, enabling a complete poloidal cross-section of the plasma to be observed. From these, a radial profile of the soft X-ray emission is constructed and it is this profile that is compared with the simulations. A 250μm, Be filter was used, giving a low energy cut-off of ~2.0keV. The estimated error in the measurement is ~5 to 10%. No division of the soft X-ray emission into its component parts is made, the comparison necessarily being with the sum of the Ni and C components.

Finally, electron density and temperature profiles are required as input to the transport simulations. These were measured by a 7 channel interferometer operating in the far infrared at a wavelength of 195μm (Braithwaite *et al*. 1989) and by an Electron Cyclotron Emission (ECE) Michelson interferometer (Bartlett *et al*. 1987), respectively. The accuracy of the profiles away from the plasma edge is typically ±10%; close to the edge, the uncertainties are expected to be larger. In addition, data from a high temporal resolution ECE grating polychromator (Bartlett *et al*. 1987) are used to give information on fast events such as sawteeth.

3. THE LINT METHOD

The Line Intensity Normalization Technique (LINT) is an empirical technique that relates VUV and XUV spectroscopic data to elemental components of radiated powers and Z_{eff}, the latter enabling the impurity concentrations to be derived. Measured spectral line intensities, one for each impurity element, are linearly scaled so as to represent the power radiated by all ionization stages of the element. This is achieved by adjusting the scalings until the sum of all the elemental components matches the total radiated power as measured by bolometry, essentially

$$P_{radBOLO}(t) - \sum_{element} c_{Pelem} I_{elem}(t)$$

being minimized, where $P_{radBOLO}(t)$ is the bolometric measurement of the total P_{rad}, c_{Pelem} is a radiated power coefficient appropriate to each impurity element and $I_{elem}(t)$ is a representative

line intensity for each element. The sum is carried out for all the impurity elements. In the case of the Z_{eff} components, each spectral line intensity, as well as being scaled linearly, is divided by a measure of n_e^2 so as to represent the impurity concentration. The volume averaged n_e has routinely been used in the JET analysis. The concentrations are then converted to Z_{eff} components and the significant components are summed. The sum is matched to the Z_{eff} as determined from visible bremsstrahlung measurements, here

$$Z_{effvisbrem}(t) - 1 - \sum_{element} \frac{c_{Zelem} I_{elem}(t)}{\langle \bar{n}_e(t) \rangle^2} \bar{Z}_{charge} (\bar{Z}_{charge} - 1)$$

being minimized. $Z_{effvisbrem}(t)$ is the Z_{eff} determined from visible bremsstrahlung measurements, c_{Zelem} a Z_{eff} coefficient for a particular element and $\bar{Z}_{charge}$ an average charge state of the more central ionization stages of each element. This will equal Z in the case of low Z elements. When dealing with the Z_{eff} it is important to include the contribution of the fuel, here assumed to be a H isotope (Z = 1). In summing the radiated power components, the contribution of the fuel is usually so small that it can be neglected. These procedures are carried out for a sequence of discharges, for which the scaling coefficients are assumed constant, the optimization being performed for the whole sequence. In cases where there are only two or three important components, all of which vary significantly, the normalization coefficients can be determined from a single pulse.

The method relies on the absolute calibration of the bolometers and visible spectroscopic diagnostics. Their calibrations can be determined more accurately than is easily achieved for the VUV and XUV spectrometers used. An example is illustrated in figure 2, figure 2a showing the radiated power components for a 3MA, D discharge, pulse 19620, and comparing their sum with the bolometric measurement of the total radiated power. In this pulse, the Ion Cyclotron Resonance Heating (ICRH) tripped on reaching 11MW, falling in steps to 3.5MW as illustrated in the figure. It can be seen that there is good agreement between the component sum and the measured total radiated power despite the sudden and significant change in the radiation.

Figure 2b shows the corresponding components of the Z_{eff} from which the concentrations are determined. Their sum is compared with the measurements of Z_{eff} derived from the visible bremsstrahlung observations. The result is a spatially averaged measure of the impurity concentrations that, like the Z_{eff} to which the components are fitted, is more indicative of the concentrations in the central region of the plasma where n_e is higher.

In deriving the radiated power components, no allowance can be made for spatial asymmetries in the radiation, since a single near-horizontal line of sight, close to the vessel midplane, is used for the spectroscopic measurements. However, in general this is not thought to be too serious a disadvantage, in that the H-like emission from even the lowest Z element considered, Be, is largely symmetrized. Indeed, there is evidence that better fits are obtained to

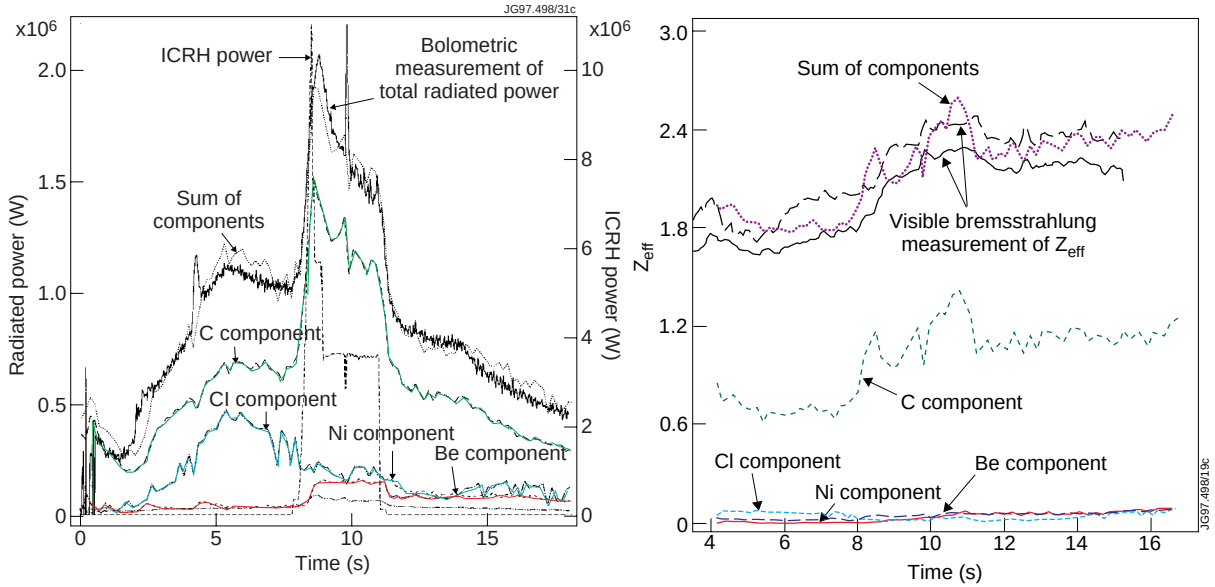

Figure 2. Elemental a) P_{rad} components, the component sum and the total radiated power and b) components of Z_{eff} and their sum and Z_{eff} measurements for pulse 19620. The ICRH power is illustrated in figure 2a) and can be seen to trip after reaching 11MW.

the total radiated power, which is derived by summing the radiation recorded along a number of vertical lines of sight and therefore involves some smoothing, than to individual bolometer channels in the horizontal midplane, whose signal can be influenced by localized asymmetric emission from the plasma edge.

3.1. The choice of spectral lines

An advantage of the LINT method is that it is possible to represent the power radiated by an element or its impurity concentration by using just one spectral line for each element. This facilitates the processing of large numbers of pulses. The choice of this line depends both on considerations of atomic physics and plasma behaviour, as well as on instrumental limitations of the spectral measurements, such as the wavelength ranges that can be observed at any one time and the spectrometers' spectral resolution. Whenever possible, a strong transition to the ground state of the ionization stage is chosen. This ensures that the excited population in the upper level of the transition is strongly coupled to that of the ground state; the latter contains most of the population of the ionization stage at the low electron densities typical of tokamak plasmas (n_e ~10^{18} - 5x$10^{19}$$m^{-3}$). For example, the population of the $2s2p\,^1P_1$ state of NiXXV, the upper level of the most intense VUV NiXXV transition, is ~10^{-5} to 10^{-6} of that of the $2s^2\,^1S_0$ ground state.

For low Z elements, such as Be, C and O, the Lyman-α transition of the element is preferred; this is the strongest transition of the radially innermost ionization stage of these elements emitting passive radiation. Evidence will be presented in section 4.2 that suggests that the H-like ionization stage of these low Z elements often accounts for the most significant part of the radiation emitted by the element. This is thought due to the significant fall in the electron density as the edge transport barrier neighbouring the Last Closed Flux Surface (LCFS) is crossed

(Erents *et al*. 1987), the emission shell of the H-like ionization stage of low Z elements lying within the LCFS.

For the higher Z elements that are common impurities in JET, like Cl, Cr, Fe and Ni, the choice of line depends both on the radial location of the emission and on the atomic physics. Spectral lines that are emitted from either the plasma edge or from the plasma centre are unsatisfactory. It is found that lines emitted from just inside the LCFS are not representative of the impurity behaviour in the bulk plasma. On the other hand, the intensity of radiation emitted from the plasma centre is particularly sensitive to the electron temperature, which determines the ionization balance in the near-coronal conditions expected in this region of the plasma where transport effects are small. The intensity of such a line is therefore representative not only of the bulk impurity concentration, but also of the abundance of the central ionization stage, which can vary significantly with modest changes in the central value of T_e.

Ionization stages whose emission shells have a limited spatial extent away from the plasma centre are preferred. For these ionization stages, changes in the electron temperature result in a movement of the emission shell to different radial locations without large changes in the ion's abundance. As T_e changes, the shell will move to regions of higher or lower n_e; it should be noted that, when calculating the radiated power, the local value of n_e is accounted for precisely in the low density tokamak plasmas, since both the line intensities and the total radiation from the ionization stage are proportional to n_e. Both the Li- and Be-like ionization stages of the higher Z elements give rise to intense lines falling in the VUV spectral region. Lines from both of these stages have been successfully used for Cl. However, the higher ionization potentials of the metals Cr, Fe and Ni, ~2keV, mean that the Li-like stage can have a wide spatial extent. The central value of T_e achieved in JET can vary from ~2 to 15keV and, therefore, the Li-like stage reaches the plasma centre in the lower temperature discharges. It follows that the Be-like stage is the more suitable.

Another consideration for the higher Z elements is that the sensitivity of the line intensity to T_e can be further minimized by using lines due to $\Delta n = 0$ rather than $\Delta n = 1$ transitions. The former, which for elements such as Cl, Cr, Fe and Ni occur in the VUV and XUV spectral regions between wavelengths of 80 and 450Å, have transition energies that are significantly lower than the T_e of the plasma region from which the radiation is emitted; in contrast, the larger energies of the $\Delta n = 1$ transitions can be comparable to T_e. The excited population within an ionization stage is dependent on the electron impact excitation cross-section and for the $\Delta n = 0$ transitions the temperature dependent exponential term in the cross-section is ~1, thus reducing its dependence.

The preferred transitions used to represent the elements commonly found in the JET plasma are listed in table 1. The wide use made of these transitions justifies them being regarded as well tested. From time to time, it has been necessary to use other transitions. Examples are the Li-like transition of Ni at 165.40Å or the Balmer-α transition of O at 102.4Å, when, respectively,

the Be-like Ni and the O, Lyman-α transitions could not be observed. On another occasion, the detector saturated for the ClXIV line at 237.81Å and the ClXIII line at 202.10Å was employed instead. The use of these alternative lines permitted an analysis to be made, although the fit was poorer and the analysis less precise.

Table 1. The preferred spectral lines used in the LINT method.

Element	Ion	Wavelength (Å)	Transition
Be	BeIV	75.93	$1s\ ^2S_{1/2}$ - $2p\ ^2P_{3/2,1/2}$
C	CVI	33.74	$1s\ ^2S_{1/2}$ - $2p\ ^2P_{3/2,\ 1/2}$
N	NVII	24.78	$1s\ ^2S_{1/2}$ - $2p\ ^2P_{3/2,1/2}$
O	OVIII	18.97	$1s\ ^2S_{1/2}$ - $2p\ ^2P_{3/2,1/2}$
Cl	ClXV	415.50	$2s\ ^2S_{1/2}$ - $2p\ ^2P_{1/2}$
Cl	ClXIV	237.81	$2s^2\ ^1S_0$ - $2s2p\ ^1P_1$
Ar	ArXVI	353.92	$2s\ ^2S_{1/2}$ - $2p\ ^2P_{3/2}$
Ar	ArXV	221.15	$2s^2\ ^1S_0$ - $2s2p\ ^1P_1$
Cr	CrXXI	149.89	$2s^2\ ^1S_0$ - $2s2p\ ^1P_1$
Mn	MnXXII	141.09	$2s^2\ ^1S_0$ - $2s2p\ ^1P_1$
Fe	FeXXIII	132.92	$2s^2\ ^1S_0$ - $2s2p\ ^1P_1$
Ni	NiXXV	118.00	$2s^2\ ^1S_0$ - $2s2p\ ^1P_1$
Cu	CuXXVI	111.18	$2s^2\ ^1S_0$ - $2s2p\ ^1P_1$

3.2. The Radiated Power and Z_{eff} Coefficients

The most valuable simplification and surprising feature of the LINT method is the use of multiplying radiated power and Z_{eff} coefficients that remain constant throughout a pulse in order to convert the measured line intensities to elemental radiated power components and concentrations. In the case of the latter, the line intensity is also divided by the square of an average value of n_e, such as the volume averaged electron density, before being converted into a Z_{eff} component by accounting for the charge state. An initial heuristic estimate is made of the coefficients and the calculated components are then summed and matched to the total radiated power or Z_{eff} by adjusting the coefficients, generally for a series of discharges.

If there are only two or three elements giving rise to significant contributions to P_{rad} or to the Z_{eff} and there is a clear variation in the impurity behaviour throughout a discharge, the coefficients can be derived from a single pulse. The larger the number of significant components and the more uniform the impurity behaviour, the more pulses are required to obtain a complete set of coefficients. Whenever possible, the coefficients are checked by a further application to subsequent discharges. Usually, the derived coefficients will remain valid for the rest

of an experimental programme. Such a programme on JET typically lasts from one half to two days. The coefficients used to generate the components shown in figure 2a were derived not from pulse 19620 and its neighbours, but from earlier pulses in the experimental programme.

Figures 3a to 3d show the radiated power coefficients used for Be, C, Cl and Ni, respectively, throughout the September/October 1990 campaign, during which ~1500 discharges were run. During this period of operations, the two belt limiters installed in the JET machine were made of Be and CFC tiles covered the inner wall and protected the vessel at the X-point strike points. The ICRH antenna screens were also constructed of Be. Cl was a significant contaminant of the machine and there were occasional influxes of Ni originating from the vessel walls. Each coefficient is for a range of pulses subsequent to the abscissa and applying until a new coefficient is indicated. For example, in figure 3a the Be coefficients for pulses 22077, 22188, 22241, 22316, etc, correspond to the start of new experimental programmes and they apply to most or all of the pulses in those programmes.

During some periods the contribution of a particular element was so small that the coefficient could not be determined; this occurred especially for Ni and the existing coefficient was assumed to apply. It was found that the initial level of C was particularly low, so that no coefficient for C was available until pulse 22300. There were a number of short periods when a different grating, the 450g.mm^{-1} grating rather than the 2105g.mm^{-1}, was used for the VUV measurements, this affecting the Cl and Ni coefficients. In the case of Cl (figure 3c), different spectral lines were used when the grating was changed, whereas the same line was used to monitor Ni (figure 3d), but the sensitivity of the gratings differed, this requiring a change in the coefficient. Changes in the coefficients can occur when a different toroidal field is used as, for example, after pulse 22291 and pulse 22296, when the toroidal field was changed from 2.8 to 3.3T and then to 1.7T. It appears that it is the magnetic fields and their effect on the bulk plasma profiles that is important, since different coefficients can be required when the plasma shaping is modified during a single experimental programme, for example after pulse 22259. It can be seen from figure 3 that the variation in the coefficients throughout the whole of this period of operations for each low Z element is ~3, whereas for higher Z elements it is larger, being ~5.

The LINT method relies on the similarity of the relationships between the T_e and n_e profiles and of their relationship with the spatial emission region of the characteristic ion stage throughout an experimental programme. That constant radiated power and Z_{eff} coefficients, independent of T_e and n_e, can be used to give satisfactory results even throughout one pulse is completely unexpected and an important result. For example, the central value of T_e in pulse 19620, which is illustrated in figure 2, varies from a few hundred eV at the beginning of the pulse to 7keV at the peak of the additional heating and the axial density rises to 4.7x10^{19}m^{-3}; despite this wide variation in temperature and density the same constant coefficients are used throughout the pulse. It is believed that the gradients of T_e and n_e and their relationship are more important in determining the coefficients than T_e and n_e themselves, although the full parametric

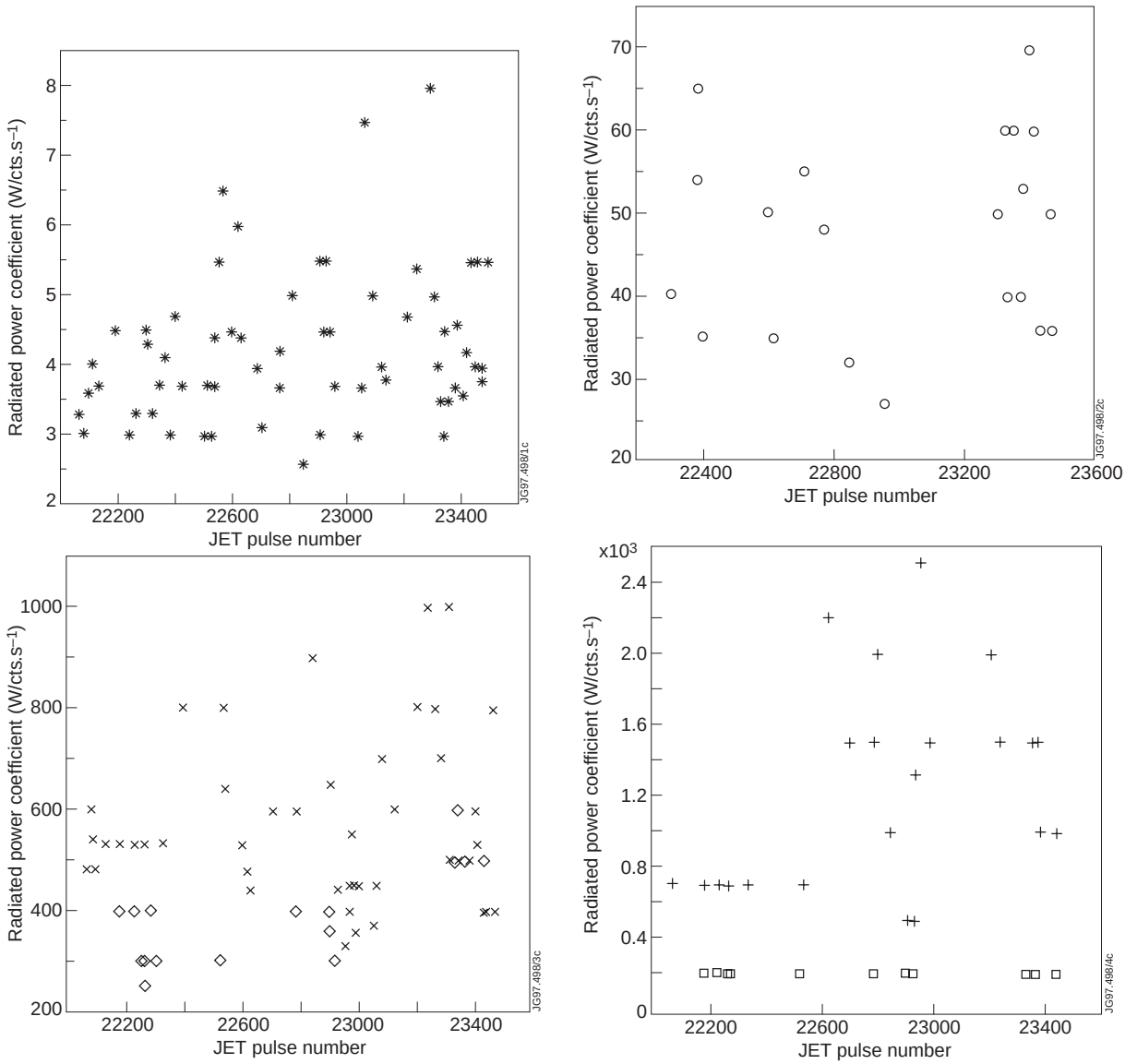

Figure 3. Radiated power coefficients used to convert a) the Be, 75.93Å, Lyman-α spectral line intensity (∗), b) the C, 33.74Å, Lyman-α line intensity (o), c) the ClXIV, 237.81Å (x) and ClXV, 415.50Å (◊) line intensities and d) the NiXXV, 118.00Å line intensity, measured with the 2105g.mm^{-1} (+) and 450g.mm^{-1} (□)gratings to radiated power components as a function of pulse number.

dependence of the coefficients is not as yet understood. Clearly, geometric factors such as the volume of the emitting plasma must be one factor determining the P_{rad} coefficients and preliminary correlations have been found between the P_{rad} coefficients and different impurity levels, a high concentration of a particular impurity affecting the temperature profile. The success of the LINT method in limiter discharges, which essentially depends on the stability of the P_{rad} and Z_{eff} coefficients, must be related to the profile consistency of the T_e profiles, such a consistency also influencing the transport within the plasma (Taroni and Tibone, 1986).

3.3. The Accuracy of the LINT method

The accuracy with which the elemental components of the radiated power can be determined is usually higher than that of the impurity concentrations. The typical accuracy of the bolometer measurements to which the spectroscopic measurements are fitted is better than 10%. As can be seen in figure 2a, the sum of the components agrees overall with the bolometric measurement of the total radiated power to within 10%. The largest components will, therefore, have a similar relative error and a somewhat larger, better than 14%, absolute error, this being typical of many of the analyses. It is noted that this is not much more than the measurement accuracy of the time histories of line intensities in the VUV and XUV spectrum. For an intense line, well-separated from its neighbours, the line integration can be performed typically to an accuracy of 5 to 10%, there being comparatively few pixels, ~7, in the central peak of the line profiles of the VUV spectral features. Clearly the error in the weaker radiated power components will be larger than ~14%, because of the difficulty in determining their coefficients.

The accuracy with which the Z_{eff} components and, hence, concentrations can be determined is generally poorer for several reasons. In part, it is due to the use of an averaged value of n_e, which may be inappropriate for the position of the emission shell. Further, the method requires the radial profile of the impurity concentration to be reasonably uniform. Severe changes in this profile could lead to the impurity concentration at the emission shell of the monitored line deviating significantly from the concentration in the plasma region of high n_e, from which the bremsstrahlung used for the measurement of the Z_{eff} is emitted. A poor match between the component sum and the measured Z_{eff} during the current ramp and decay phases of the discharge is always observed and generally more care is needed with the validation of the derived concentrations. Although the higher Z elements can make a significant contribution to the radiated power, their concentration is nevertheless low and, consequently, their contribution to the Z_{eff} is usually small. The determination of their concentrations by the LINT method is more difficult, although as the simulations described in section 4 show is still possible. The accuracy of the Z_{eff} measurement derived from the visible bremsstrahlung is typically ±20% and it is estimated that the impurity concentrations of the elements giving rise to the largest Z_{eff} components can be determined to within ±30%, an estimate consistent with the simulations.

3.4. Examples of the application of the LINT method

The LINT method offers a simple and reliable procedure for dealing with the most significant impurities in a discharge. Confidence in the P_{rad} components and concentrations stems from the match between the radiated power and Z_{eff} component sums with independent diagnostic measurements, this providing an immediate and convincing check. This ensures that all the significant impurities are included and indicates the presence of unexpected elements in the plasma, which can be identified from the available spectra. Because the radiated power fits are the more

accurate and the medium and higher Z impurities may have a large radiated power component, but only make a small contribution to the Z_{eff}, the P_{rad} analysis is carried out first in practice and acts as a reliable assessment of the impurities intrinsic to the discharge.

The method can be applied to a wide range of plasma parameters, including different plasma currents, all the temperatures and densities that have been encountered on JET and additionally heated discharges. As an example, figure 4 illustrates the radiated power components, their sum and the bolometric measurement of the total radiated power for a 3MA, D discharge, pulse 22093, with additional heating, 2.9MW of ICRH, 2.7MW of Neutral Beam Injection (NBI) and 0.7MW of Lower Hybrid Current Drive (LHCD). This pulse was run in 1990 when the limiters were Be and it can be seen that nearly all the radiation is due to this element. The reconstruction of the bolometer time history, in this case almost entirely from a single element represented by one spectral line, emphasizes that the independence of the radiated power coefficient from T_e and n_e is not chance; rather it must be crucial to a full understanding of the physics of the transport of impurities and the radiation processes. In this pulse, the peak T_e rises to 8keV and the axial n_e to $2.7 \times 10^{19} m^{-3}$.

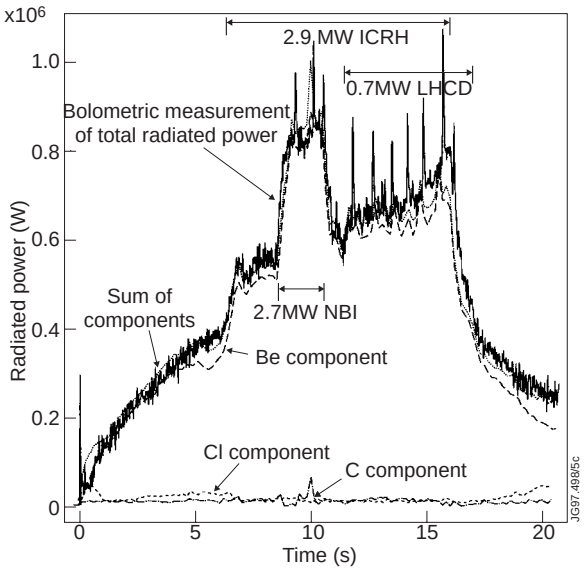

Figure 4. Elemental P_{rad} components, their sum and the total radiated power for pulse 22093, which has low power NBI, ICRH and LHCD and in which Be dominates the radiated power.

Similar traces are shown in figure 5 for a neighbouring 3MA discharge, pulse 22083, which has 3.4MW of ICRH and 2.6MW of NBI additional heating. In this case, Cl also contributes significantly to the radiated power and is responsible for a large (~1MW) influx at ~20s. It can be seen that the radiation due to Be, the element from which the limiters and antenna screens were constructed, rises at the time of the additional heating, whereas the Cl component falls. This impurity behaviour is typical of many discharges during the 1990 campaign, although in some pulses the fall in the higher Z element's component is less marked. Figure 6 shows component powers for pulse 20499, another 3MA discharge with up to 3MW of ICRH, run as a conditioning pulse at the beginning of the September 1989 operations. Early in this pulse the plasma density oscillates, this being a particularly severe test of the LINT method. As in pulse 22083, Be and Cl are the main radiators, the total radiated power being reasonably well matched.

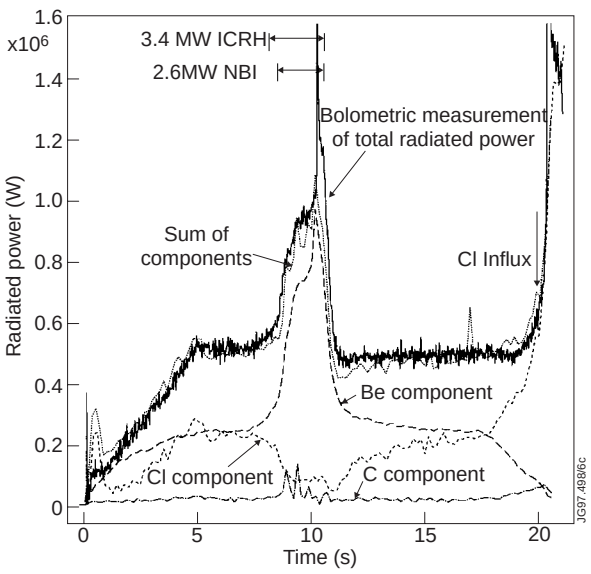

Figure 5. Elemental P_{rad} components, their sum and the total radiated power for pulse 22083, showing the behaviour of Be and Cl during additional heating and an impurity influx due to Cl.

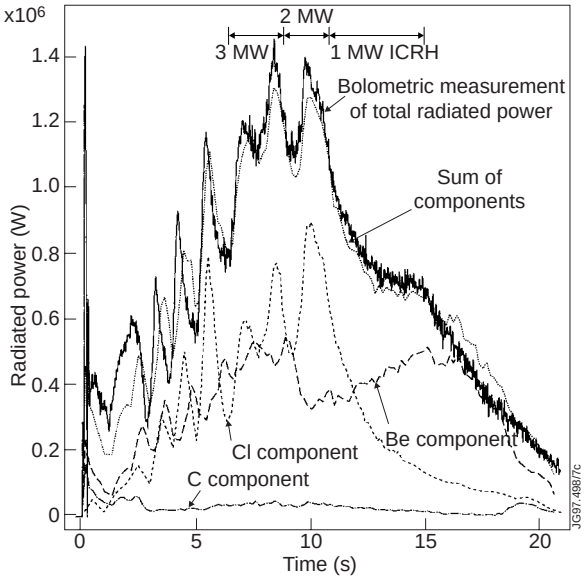

Figure 6. Elemental P_{rad} components, their sum and the total radiated power for pulse 20499. The oscillations in the radiated power result from changes in the plasma density.

Operating the JET machine at high densities produces a very different impurity behaviour. Figure 7a and 7b illustrate the empirical components, their sum and the measurement of the total P_{rad} for ohmic and additionally heated, 4MA, D fuelled density limit discharges, pulses 20845 and 20849, respectively. 5.0MW of ICRH and 7.8MW of NBI were applied to the latter. A line-averaged density of $5.9 \times 10^{19} m^{-3}$ was reached in the ohmic case and this was doubled by the application of additional heating, a line-averaged density of $1.2 \times 10^{20} m^{-3}$ being achieved. These discharges were run soon after the Be belt limiters and Be antenna screens were installed in JET,

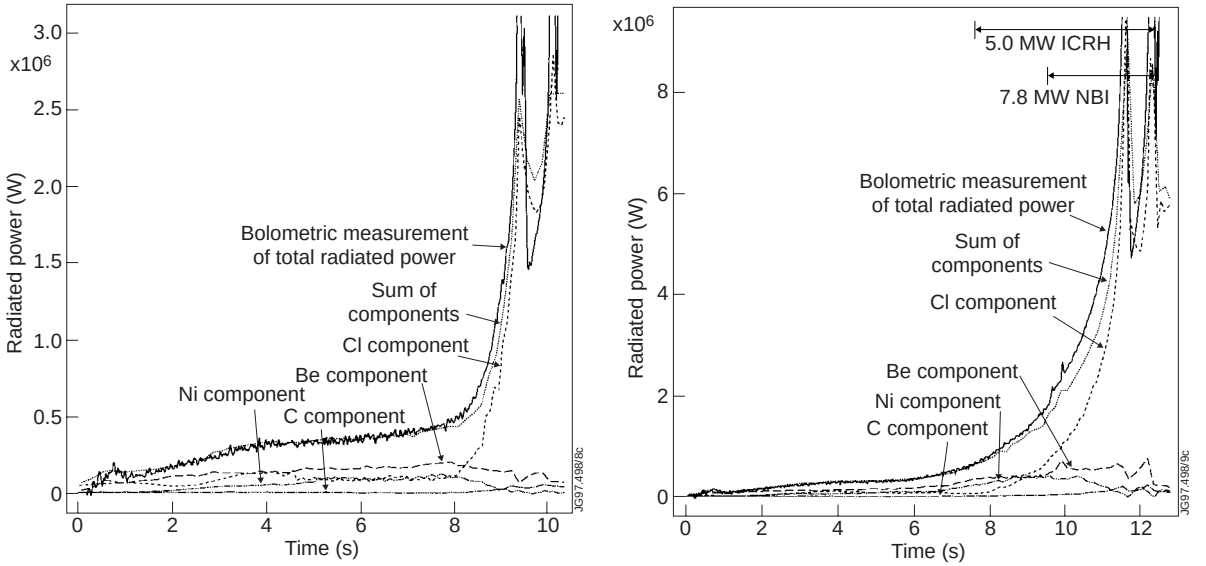

Figure 7. Elemental P_{rad} components, their sum and the total radiated power for a) the ohmic density limit pulse 20845 and b) the additionally heated density limit pulse 20849, showing the importance of the medium Z element, Cl, as the density limit is approached.

the presence of Be in the machine resulting in a soft, MARFEing (Lipschultz *et al*. 1984) termination rather than the hard density limit disruption found when all the plasma-facing surfaces are C. In these pulses, the errors are larger than in some of the less extreme examples, although the analysis clearly shows the importance of the Cl contribution to the total radiated power as the density limit is approached. That the method can allow absolute accuracies of ~15% to be achieved from VUV and XUV spectroscopic measurements is clearly highly advantageous, even if relying on cross calibrations with the bolometers and visible spectroscopy.

3.5. The limitations of the method

The main limitation of the LINT method is the accuracy with which weak components can be treated. The smaller the contribution of a component to the radiated power or Z_{eff}, the more difficult it is to obtain a reliable value for its coefficient. Nevertheless, it is usually the elements giving rise to the more significant contributions that are of most importance and interest.

Assuming that all the impurities in a discharge have been correctly accounted for, discrepancies between the component sum and the measured total radiated power still arise if there are poloidal asymmetries in the spatial distribution of the radiation, such as a MARFE, or if there are influxes, either discrete or near-continuous. During a transient event such as an impurity influx, there is an excess of population in the low ionization stages of the element, both because of the time taken for the ions to diffuse into the centre of the plasma and for the ionization process itself. For the heavier elements, ionization occurs many times and ions moving towards the plasma centre can reach higher temperature regions than would be expected under steady-state conditions; this distorts the populations within each ionization stage. The higher temperature regions normally have a higher density, this leading to increased radiation with the result that the measured radiated power can exceed that determined by the empirical method, because of emission from these low ionization stages.

4. VERIFICATION OF THE LINT METHOD USING TRANSPORT SIMULATIONS

In order to provide independent confirmation of the empirically derived impurity concentrations and elemental radiated power components and to demonstrate their usefulness in detailed transport analyses, transport simulations have been carried out for the intrinsic C and Ni impurities in three L-mode discharges, pulses 13728, 13734 and 13738, chosen from a sequence of 3.5MA discharges with a toroidal field of 3.4T in a high power, ICRH campaign. The plasma in the second pulse detaches after 10s and the Ni concentration in the third is high enough to cause a disruption. The discharges have D fuel with a ^{3}He minority, which allows between 9 and 10MW of ICRH power to be coupled to the plasma.

At the time the discharges were run (December 1987), most plasma facing surfaces were C, the main exception being the ICRH antenna screens, which were made of Ni. The latter element was found to be an important contaminant and had the effect of gettering O, suppress-

ing the plasma O content to the extent that it was no longer significant. Consequently, C and Ni are the only important impurities in these pulses, this leading to particularly satisfactory and reliable fits of the radiated power and Z_{eff} component sums when applying the LINT method. The discharges belong to one of the simplest regimes of interest both in terms of transport and impurity behaviour and are therefore ideally suited to this study.

Table 2. Plasma parameters of the pulses modelled.

Pulse	13728	13734	13738
Time of simulation (s)	9 - 10	8 - 10	7 - 9
Plasma Current (MA)	3.5	3.5	3.5
Maximum Te (keV)	10.3	12.0	11.0
Maximum ne (m^{-3})	4.0 x 10^{19}	3.8 x 10^{19}	4.6 x 10^{19}
ICRH Power (MW)	9.0	10.0	9.7
Stored Energy (MJ)	3.5	5.1	4.6
Radiated Power(MW)	4.8	5.4	6.2 - 8.1
Z_{eff}	5.5	6.2	5.3 - 5.7

The analysis is made for the L-mode phase of the pulse, after the ICRH has reached full power and is approximately constant. At this time, the Ni emission is most intense and therefore can be measured with least error. Sawteeth lead to a redistribution of particles in the central region of the plasma and, consequently, to avoid any confusion, sawteeth-free periods of the discharge are used in the comparison with the experimental data. Table 2 gives the discharge times for which the simulations are carried out, together with pertinent plasma parameters. Time histories of the plasma parameters for pulse 13738 are shown in figure 8.

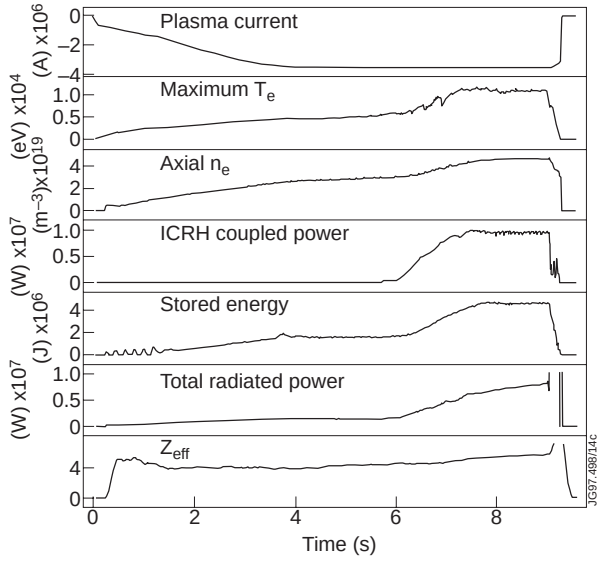

Figure 8. Time histories of the main plasma parameters for pulse 13738, which was analysed in the impurity transport modelling.

Simulations of intrinsic impurities usually make comparisons with the total radiated power or Z_{eff}. In this case, the LINT elemental components and concentrations are used. The division of the bolometric measurement of the radiated power and the Z_{eff} derived from the visible bremsstrahlung into elemental components by the LINT method is illustrated for each of the pulses in figures 9 to 11. The discrepancy observed between the Z_{eff} and the components' sum from 10.2s in pulse 13734, figure 10b, which is after the time of interest for the simulations, is due to the plasma detachment. In figure 10a, it can be seen that the

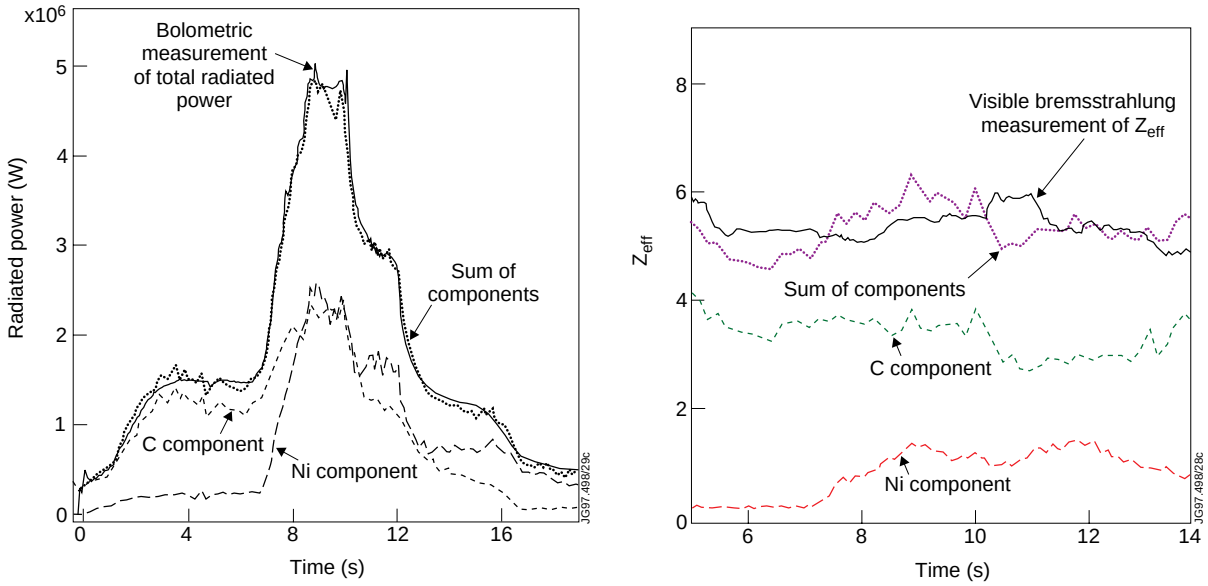

Figure 9. a) Elemental P_{rad} components, the components' sum and the total radiated power and b) Z_{eff} measurement and components of Z_{eff} together with their sum for pulse 13728, showing the contributions of the two dominant impurities, C and Ni. The transport of these impurities has been modelled.

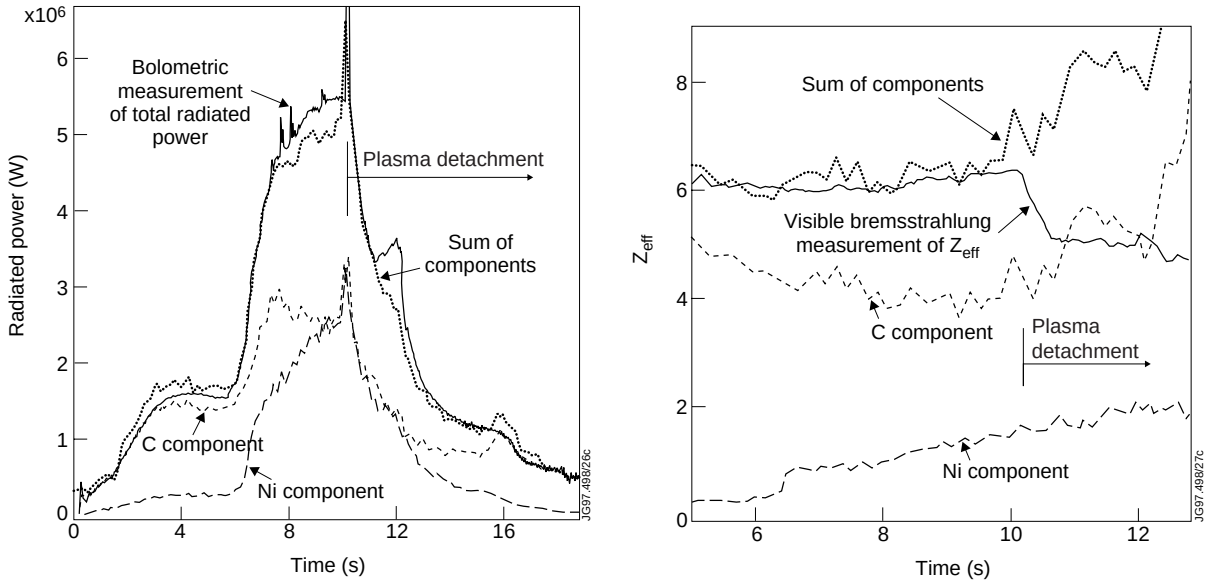

Figure 10. a) Elemental P_{rad} components, the components' sum and the total radiated power and b) Z_{eff} measurement and components of Z_{eff} together with their sum for pulse 13734, in which there is plasma detachment after 10s and for which transport modelling is presented.

derived radiated power components for this pulse nevertheless sum to give a reasonably good match to the total radiated power even during the period of the plasma detachment.

The good agreement between the components' sums and the total radiated power and Z_{eff} in these three pulses suggests the highest accuracies in the empirically derived data, which will put stringent constraints on the transport analysis. From section 3.3, these are ±15% for the elemental components of P_{rad} and ~30% in the concentrations. The emission from which the Z_{eff} is calculated depends on the function $\int n_e^2(r) T_e^{-0.5}(r) Z_{eff}(r) dr$, where r is the minor

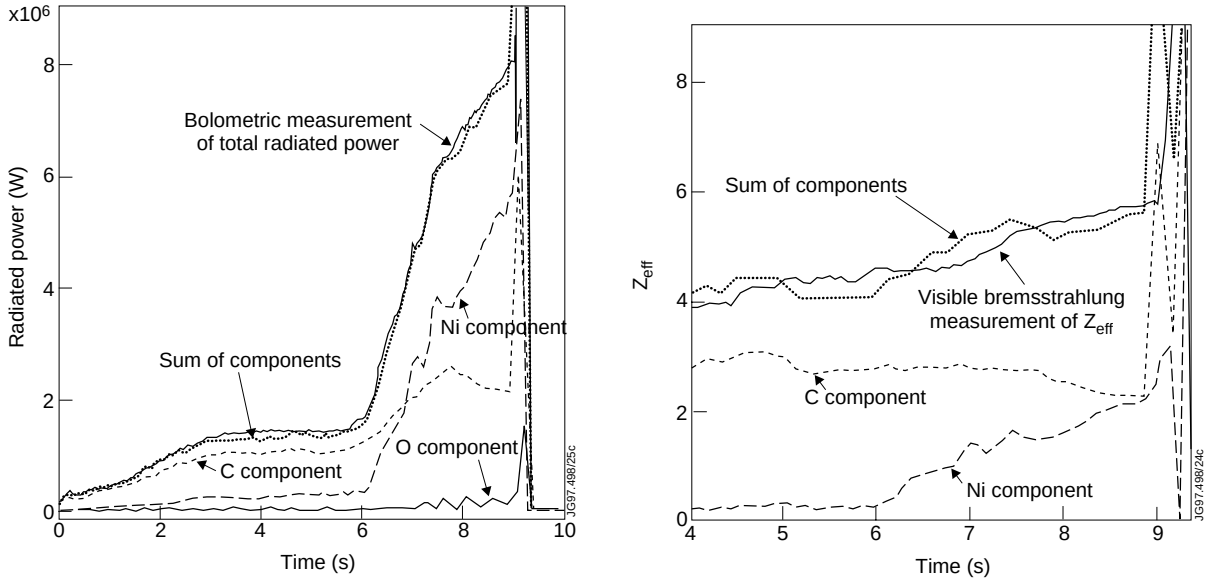

Figure 11. a) Elemental P_{rad} components, the components' sum and the total radiated power and b) Z_{eff} measurement and components of Z_{eff} together with their sum for pulse 13738, which disrupts at 9s due to the high Ni levels and for which transport modelling is presented.

radius. Consequently, a radially averaged Z_{eff} derived from this line of sight measurement will be biased towards those radii for which the integrand, $n_e^2(r)T_e^{-0.5}(r)$, is large. In these pulses, this function, although peaking at the plasma centre, is nevertheless found to be slowly varying up to a normalized minor radius of r/a ~0.6, where a is the minor radius at the LCFS. Outside this radius, the function falls away more rapidly. It follows that the impurity concentrations derived will represent a radially averaged value appropriate to the plasma region within r/a ~0.6.

4.1. The transport model

The transport simulations have been carried out using the SANCO impurity transport code (Lauro-Taroni *et al*. 1994). In this 1_-D, time-dependent code, the radial flux of impurities is described in terms of the sum of a diffusive and convective term, for each ionization stage Z,

$$\Gamma_Z(r,t) = -D(r)\nabla n_Z(r,t) + V(r)n_Z(r,t),$$

where D(r) and V(r) are the diffusion coefficient and convection velocity and $n_Z(r,t)$ is the particle density. The code takes account of the plasma geometry for the magnetic surface averages. The simulations rely on atomic physics data for two separate calculations. The first involves the use of ionization, S_Z, and recombination rates, α_Z, in the source term of the continuity equations,

$$\frac{\partial}{\partial t}n_Z(r,t) + \nabla\Gamma_Z(r,t) = -S_Z n_Z(r,t) + S_{Z-1}n_{Z-1}(r,t) - \alpha_Z n_Z(r,t) + \alpha_{Z+1}n_{Z+1}(r,t),$$

the solutions of which provide radial profiles of the particle densities for the different ionization stages. Subsequently, it is necessary to calculate the power radiated by particular spectral lines

and the total power from an ionization stage, including line radiation, recombination radiation and bremsstrahlung. The total power is then summed for all stages to give the total power radiated by the element and that emitted in the soft X-ray spectral region is determined. The atomic data are taken from the ADAS (Atomic Data and Analysis Structure) data base (von Hellermann and Summers 1993). The simulations for the two impurities were carried out independently, frictional forces between impurities being neglected.

4.2. The simulations for C

The line emission from C is localized at the edge of the JET plasma and consequently, without an active technique to diagnose more central regions, the emission from this low Z element gives little information about the central transport parameters. Nevertheless, the transport modelling for C is useful in two respects. Its contribution to the soft X-ray emission is required so that comparisons with the experimental data can be made and it suggests a feature that has an important bearing on the modelling for Ni.

In the simulations, the C influx is adjusted until agreement is found between the empirically derived and simulated C concentrations. This ensures the best calculation of the C component of the soft X-rays and one which is least sensitive to transport, the measurement of the concentration being biased towards the centre of the discharge from where the soft X-rays are emitted. In addition, the C, Lyman-α line intensity at 33.74Å, measured on the XUV instrument, for which there was no independent sensitivity calibration, was scaled to match the simulated intensity. Large discrepancies found for the absolutely calibrated CIV and CIII line intensities are consistent with these ionization stages falling within the Scrape-Off-Layer (SOL), for which the present model is inappropriate. A significant discrepancy is also found for the CV resonance line intensity at 40.27Å. The absolute sensitivity at this wavelength is similar to that at 34Å and the measured intensity is always low when compared with the simulation.

To reduce the simulated CV resonance line intensity sufficiently requires the CV emission shell to straddle the LCFS, the emission from the SOL being small due to the fall-off in n_e as the LCFS is crossed. The best agreement is found both with modifications to the measured T_e and n_e profiles, for which there is the largest uncertainties towards the plasma edge, and with the introduction of an edge transport barrier, which increases the gradients across the LCFS and further reduces the emission from the SOL. The use of such a barrier is consistent with the results of Denne-Hinnov *et al*. (1993), who model laser-ablated influxes of Fe and Ni into L-mode plasmas. Uncertainties in the profiles and transport parameters make a precise determination of the barrier in the present pulses unreliable, although it is clear that it must be large enough to have a significant effect on the impurities at the plasma edge. Neither is it possible to distinguish between a diffusive or convective barrier when dealing with the present slowly varying intrinsic impurities and the choice was made to use a convective barrier in the simulation of Ni.

Reducing the CV emission in this way leads to the CV ionization stage making a small contribution to the total radiated power. Indeed, this is expected from the reaction of the different ionization stages to an influx in pulse 13728. Intensities for the resonance or other intense spectral line from each of four C ionization stages are shown in figure 12 for this pulse. At 15.2s the plasma is moved to the inner wall. The C source in the line of sight of the spectrometers greatly increases and results in markedly different time behaviours for the line intensities from the different ionization stages. A comparison of figures 12 and 9a shows that it is the CVI line intensity, the one used in the LINT method, that best fits the bolometer data. Whereas the observed CIV and CIII emission appears to be localized, that of CVI and CV must be from largely within the LCFS, where it is more symmetrized. The resulting smoothing is consistent with the much smaller rise in the observed CVI and CV line intensities at 15.2s. If a similar hypothesis to that implicit to the empirical technique is made, that for the CVI and CV ionization stages the total radiation emitted from an ionization stage is proportional to the intensities of the resonance lines, it follows that the total radiation due to the CVI ionization stage must dominate that due to the CV and lower C ionization stages.

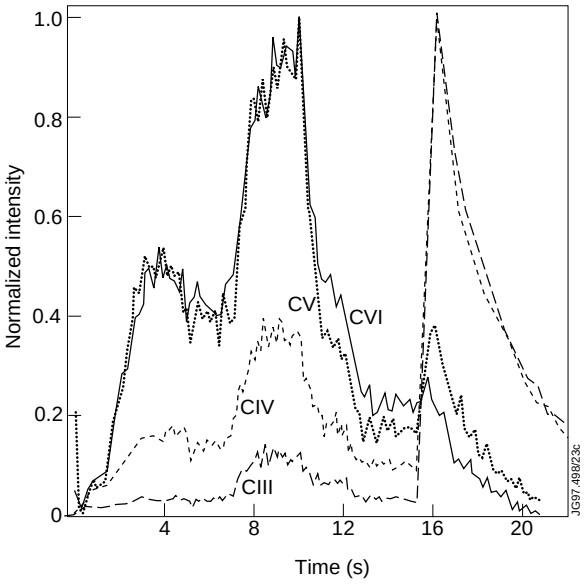

Figure 12. Time histories of the normalized CIII to CVI line intensities measured in pulse 13728, showing a C influx at 15.2s when the plasma is moved to the inner wall.

4.3. The simulations for Ni

Ni radiates line emission from all spatial locations within the plasma and is therefore a suitable element to determine radial profiles of the impurity transport parameters. It should be noted that these might only apply to similar, medium Z elements. Comparisons of the simulations with the experimental data not only provide a test of the LINT empirical method, but also enable the atomic physics data to be checked and provide confirmation of the instrumental calibrations.

All the available experimental data were compared with the simulations, although particular importance was given to the comparisons of the line-of-sight measurements of the spectral line intensities, since their calculation is expected to be the most reliable. There are six intense Ni lines in the VUV spectral region belonging to the NiXXVI, NiXXV, NiXVIII and NiXVII ionization stages, their wavelengths being indicated in figure 1. The simulated radial distribution of emission that integrates to give the line-of-sight intensities for these and other ionization stages is shown in figure 13 for pulse 13738. The innermost line emission observed is from

NiXXVI, which has a very broad emission profile centred just outside half the minor radius. As would therefore be expected, the line intensities are of most use in determining the transport parameters in the outer region of the plasma. In all the simulations, the particle influx was derived by normalizing to the line-of-sight measurement of the radially outermost line observed, the NiXVII line at 249Å.

The simulations have been carried out for a range of transport parameters as described in section 4.4, both with and without an edge transport barrier. Table 3 gives examples, one for each of the 3 pulses studied, of the ratios of the measured to simulated results for the line

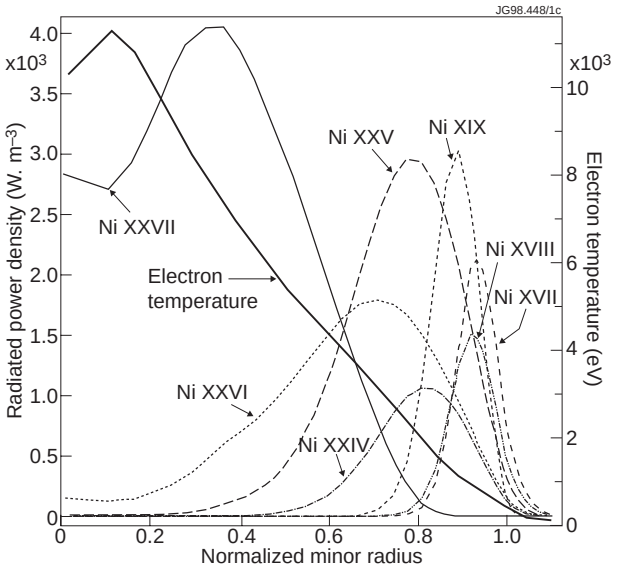

Figure 13. Radial profiles of T_e and the simulated Ni line emissions for the ionization stages neighbouring NiXVIII and NiXXV at 8.0s in pulse 13738.

Table 3. Examples of ratios of the measured to simulated line intensities, concentrations and powers for each of the pulses studied.

Pulse	13728	13734	13738
Outer D ($m^2.s^{-1}$)*	2	3	5
$\int_0^1 (x-0.96)^2 V(x)\,dx\,(m.s^{-1})^+$	-2.55 x 10^{-4}	-4.43 x 10^{-4}	-8.35 x 10^{-4}
Line Intensities			
NiXVII – 249Å	1.00	1.00	1.00
NiXVIII – 292Å	1.06	1.26 - 1.28	0.99 - 1.06
NiXVIII – 321Å	1.10	1.19 - 1.20	1.13 - 1.19
NiXXV – 118Å	0.99	0.94 - 1.10	0.84 - 0.92
NiXXVI – 165Å	Detector saturating	Detector saturating	0.87 - 0.92
NiXXVI – 234Å	0.93	0.87 - 1.07	0.87 - 1.00
Ni Concentration#	0.79	0.63 - 0.78	0.78 - 0.79
Ni Radiated Power	1.36	1.15 - 1.38	1.31 - 1.32
Soft X-rays			
r / a = 0.1	0.93	0.90 - 0.95	0.73 - 0.77
r / a = 0.6	0.61	0.55 - 0.65	0.47 - 0.54

*The diffusion coefficient for a normalized radius r / a > 0.4.

+The term for the convective edge transport barrier is discussed in section 4.4.

#An averaged ratio of the total Ni ion to electron density for r / a < 0.6.

intensities, concentrations and powers. Generally, good agreement is found between the simulated and measured line intensities, to within 20% for pulses 13728 and 13738, although somewhat poorer with discrepancies of up to 30% for pulse 13734. In particular, the measurement of the NiXVIII lines, whose emission shell is almost spatially coincident with that of NiXVII, is usually higher than the simulated value. These lines fall to longer wavelengths in the spectrum and, consequently, this discrepancy could be explained by a 10 to 15% error in the sensitivity calibration of the VUV spectrometer at wavelengths of ~300Å, the inverse sensitivity needing to be reduced. The 234Å, NiXXVI line, which is adjacent to the NiXVII line in the spectrum, agrees to within 15% in all but one of the simulations carried out. This agreement is not entirely fortuitous in that, although the optimum simulation requires a balance of all the parameters described, special weight is given to this line, because of the spectral coincidence and the radial separation of the NiXXVI and NiXVII emission shells.

In pulses 13728 and 13738, the simulated and empirically derived concentrations agree to within the expected errors, the empirical values being ~20% lower. This provides independent confirmation of the concentrations derived using the LINT method for these pulses. Near the beginning of the simulated period in pulse 13734, the discrepancy between the concentrations is ~35%, this being larger than the expected accuracy of 30%; however, in less than 0.7s the agreement is within the expected accuracy.

If the same transport parameters are assumed for C as have been derived for Ni, the contribution of the C bremsstrahlung to the soft X-ray emission is ~10 to 40% of the Ni component, uncertainties in the C contribution therefore being less important than those for Ni. Comparisons have been made between the sum of the simulated C and Ni emissions and the measured soft X-rays. In pulses 13728 and 13734, there is agreement to within 10 to 20% at the centre of the discharge; figure 14 shows profiles of the measured and simulated soft X-ray emissions for pulse 13734 at 8.5s. However, in pulse 13738, the Ni component alone at the centre of the discharge either matches or exceeds the measured soft X-ray emission, this leading to the C and Ni sum exceeding the measurement by ~10 to 30%. At intermediate radii the Ni component by itself is comparable to or in most cases exceeds the measured soft X-rays, as can be seen for pulse 13734 in figure 14. Again this discrepancy is largest for pulse 13738, the simulated Ni component approaching twice the measured emission at r/a ~0.6.

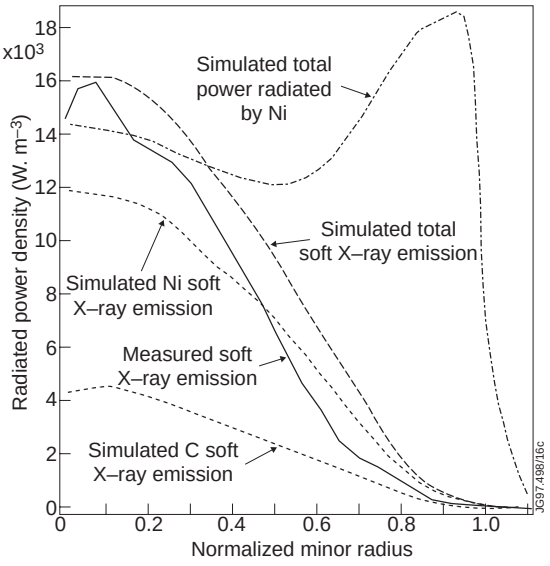

Figure 14. Radial profiles of the measured and simulated soft X-ray emissions and of the simulated total power radiated by Ni at 8.5s in pulse 13734.

In contrast, the simulated total power radiated by Ni is always smaller by between 15 to 40% than the empirically derived elemental power component. This discrepancy is larger than the expected accuracy of the LINT elemental components and therefore the simulation does not provide independent confirmation of the technique applied to the radiated powers to the accuracy expected from the internal consistency of large data sets. A radial profile of the simulated total power radiated by Ni at 8.5s in pulse 13734 is included in figure 14. It can be seen that the spectrally near-coincident NiXXVI and NiXVII lines originate from plasma regions (figure 13) for which, in one case, the soft X-ray discrepancy is largest and, in the other, the magnitude of the total radiated power is highest.

Allowing for the complexity of the transport simulations, they must be regarded as being very satisfactory, in that the noted discrepancies, chiefly in the total radiated power component and the soft X-ray emission away from the plasma centre, are at most 50%. Nevertheless, consideration has been given to possible reasons for these discrepancies. Among the factors investigated are additional radiation from the SOL, spatial asymmetries in the radiation from within the LCFS and errors in the electron temperature and density profiles, in the VUV spectrometer's sensitivity calibration and in the atomic data sets being used.

Table 4. Ratios of the measured to simulated line intensities, concentrations and powers for a case with modified edge T_e and n_e profiles.

Pulse	137328
Outer D ($m^2.s^{-1}$)*	5
$\int_0^1 (x-0.96)^2 V(x)\,dx\,(m.s^{-1})^+$	-1.23 x 10^{-3}
Line Intensities	
NiXVII – 249Å	1.00
NiXVIII – 292Å	0.83 - 0.89
NiXVIII – 321Å	0.94 - 1.01
NiXXV – 118Å	0.71 - 0.80
NiXXVI – 165Å	0.86 - 0.95
NiXXVI – 234Å	0.87 - 1.01
Ni Concentration#	0.93 - 0.94
Ni Radiated Power	1.26 - 1.32
Soft X-rays	
r / a = 0.1	0.85 - 0.88
r / a = 0.6	0.53 - 0.66

*The diffusion coefficient for a normalized radius r / a > 0.4.

+The term for the convective edge transport barrier is discussed in section 4.4.

#An averaged ratio of the total Ni ion to electron density for r / a < 0.6.

Neither additional radiation from the SOL, nor spatial asymmetries in the radiation from within the LCFS can explain the discrepancies. Further, no evidence has been found to suggest errors in the sensitivity calibration of the VUV spectrometer other than a possible 10 to 15% error at wavelengths of ~300Å as discussed above. Significant modifications to the edge T_e and n_e profiles can lead to improved overall fits between the measured data and simulations, an example being presented in table 4. This simulation, which is for pulse 13738, has the most extreme transport considered, an outer D of $5m^2.s^{-1}$. Despite some improvement in the agreement, the discrepancies for the radiated power and soft X-ray emission at r/a of 0.6 remain. The discrepancy for the radiated power is probably due to a limitation in the atomic data for intermediate ionization stages of Ni, such as NiXV to NiXXV. In no simulation was it possible to find agreement for the soft X-rays at radii away from the plasma centre. Crucially, the shape of the simulated and measured soft X-ray profiles always differ, the measured soft X-ray profile falling away more rapidly than can be explained by the simulation. This brings into question the reconstruction of the soft X-ray emission profile. Given the importance of understanding the discrepancies in the transport modelling details are presented in an appendix.

4.4. Discussion

The use of the LINT elemental radiated power components and concentrations, together with soft X-ray measurements and absolutely calibrated line intensities, puts stringent constraints on the transport modelling of the intrinsic Ni impurity, particularly for the plasma region outside r/a ~0.3. This leads to confidence in the description of the impurity transport for medium Z impurities in these pulses. The number of constraints applied means that the problem is 'overdefined', with the consequence that some discrepancies would be expected. Given the complexity of the modelling, the magnitude of the discrepancies found is regarded as being very satisfactory. It should be noted that such uncertainties do not at all limit the investigation of the edge transport parameters; these were adjusted until the same balance of agreement and disagreement was achieved in the different simulations.

The radial profile of the diffusion coefficient used in the simulations is based on those of Giannella *et al*. (1994), with an outer region of high anomalous diffusion and low central diffusion, as illustrated in figure 15 for pulse 13728. The available magnetic equilibrium data suggests that the safety factor, q, of the

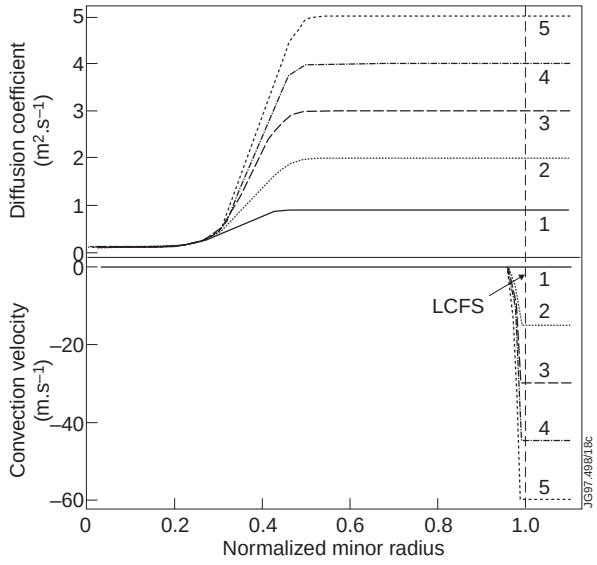

Figure 15. Radial profiles of the transport parameters, the diffusion coefficient and the convection velocity, used in 5 of the simulations for pulse 13728.

present 3.5MA discharges is similar to the 3 and 4MA pulses investigated by these authors and so a normalized radius for the transition between the low and high diffusion regions consistent with their findings of r/a of 0.3 to 0.4 was used. In fact, the modelling of the available experimental data is not especially sensitive to the precise location of this transition region and not at all to the inner diffusion coefficient. In a study of intrinsic impurities, the main effect of a lower inner diffusion coefficient is expected to be a difference in the central ion density. With a transition region at about r/a of 0.3 to 0.4, the variation in the ion density profile is at most 4%. Consequently, after some initial checks to determine the sensitivity, the transition region was fixed at r/a of 0.3 to 0.4 and the inner diffusion coefficient to ~0.1$m^2.s^{-1}$ in all the simulations. Various modifications to the shape of the outer diffusion coefficient were tested, but no justification was found for using anything but a constant outer value in this modelling.

Giannella *et al*. use the conventional form for the radial dependence of the convection velocity, together with a peaking factor, S,

$$V(r) = -2S\,\frac{D(r)\,r}{a^2}.$$

In most of their simulations, S is taken to be 1. In the present analysis, such a convection velocity gives too strong an inwards particle drift and the most satisfactory agreement with experiment was obtained by using a negligible convection velocity throughout most of the plasma. In particular, it is noted that the agreement between the 234 and 249Å lines, which was discussed in section 2.2, is no longer within ~10%. The radial profiles of the convection velocity used in the simulations for pulse 13728 are shown in figure 15.

The particle influx in the present simulations was determined by normalizing to the measured 249Å, NiXVII line of sight spectral line intensity. The NiXVII ion density profile is centred on a radius of r/a of ~0.96 and, consequently, it is not possible to determine the magnitude of any edge transport barrier, since the NiXVII falls largely within the barrier. The barrier is required in order to obtain the best agreement in the simulation of the intrinsic C impurity in these pulses and is also suggested by the modelling of Denne-Hinnov *et al*. (1993), who use a combined diffusive and convective barrier in contrast to the present use of a convective only barrier.

Nevertheless, the introduction of an edge barrier has a significant effect on the particle balance within the plasma, the inward convective barrier confining particles and the diffusion process within the bulk of the plasma tending to aid the removal of the intrinsic impurity particles. A strong convective edge barrier, therefore, requires a higher outer diffusion coefficient to balance the impurity particle inventory. Since the NiXVII line emission to which the simulation is normalized has a significant radial extent, the shape of the edge barrier must be considered. Barriers for which the integral $\int_0^1 (x-0.96)^2\,V(x)\,dx$ is the same were found to be equivalent in that they confine particles to the same extent, requiring the same outer diffusion coefficient. In

this integral, x is the dimensionless, normalized minor radius, r/a, the integral being evaluated from the plasma centre to the LCFS. The value x = 0.96 corresponds to the peak of the NiXVII ion density profile. In the simulations, a range of outer diffusion coefficients were chosen, these varying from ~1$m^2.s^{-1}$, which requires no edge transport barrier, up to an extreme value of 5$m^2.s^{-1}$. The convection velocity away from the plasma edge was taken to be negligible (S = 0) and the appropriate edge barrier determined. The results for the three pulses that have been modelled follow a linear relationship

$$D = K\int_0^1 (x - 0.96)^2 V(x)\,dx + D_0,$$

where the constants K and D_0 are given in table 5. It should be noted that none of the experimental measurements used in this analysis have an exceptionally good spatial resolution at the plasma edge. Consequently, the form of the edge barrier derived in this modelling is thought to depend largely on the SANCO model itself, particularly the shape of the NiXVII ion density profile, rather than representing any underlying physics relating to the barrier.

Table 5. Values found for the parameters determining the linear relationship of the particle balance.

Pulse	13728	13734	13738
K (m)	-3990	-4310	-4770
D_0 ($m^2.s^{-1}$)	0.94	1.06	1.02

5. CONCLUSIONS

A novel, empirical procedure, the LINT method, used to determine elemental components of radiated power and impurity concentrations is described. This method involves the separation of the bolometric measurement of the total radiated power and the Z_{eff} as determined from observations of visible bremsstrahlung into elemental component parts, each due to an intrinsic plasma impurity. This is achieved through the use of VUV and XUV spectral features. Particular spectral line intensities are related to each elemental component by a constant coefficient, an allowance for density being made in the case of the Z_{eff} components. Unexpectedly, the coefficients are independent of T_e and n_e. This is seen most clearly for the elemental P_{rad} components where a single constant coefficient is used for each element throughout a discharge, despite the wide variations that occur in both parameters. This independence has important implications for the understanding of how the impurity transport and atomic processes combine to give the radiation emitted from a tokamak plasma.

The method relies on the absolute calibrations of the bolometers and visible spectrometers. The technique has the advantage of simplicity, allowing larger numbers of pulses to be processed than would be possible if detailed transport modelling was required for each pulse. It has been extensively applied to limiter discharges run in the JET tokamak. Since the method in-

volves comparisons with independent diagnostics, it also has the advantage of reliability in that discrepancies are immediately obvious. When good agreement with other diagnostics is found, the elemental P_{rad} components for the most significant elements in the plasma can be determined to within an accuracy of ±15%. Trace elements can also be treated, but with increased errors. The concentrations represent a spatial average of the more central plasma region and in the best cases can be accurate to within ±30%.

These data have numerous uses both during plasma operations, as part of an intershot analysis, and in later, more detailed studies. One application is to transport modelling and the value of the stringent conditions that the LINT results impose on the model is illustrated by simulations using the SANCO, 1_-D diffusive convective transport code of three L-mode, D discharges, to which 9 to 10MW of ICRH was applied. The simulations provide independent confirmation of the LINT concentrations. However, the complexity of the modelling is such that the discrepancies between the empirically derived and simulated radiated powers are larger than the expected accuracy of the empirically determined data. The analysis is therefore unable to validate the elemental P_{rad} components to the accuracy already deduced from the internal consistency within large data sets.

The modelled pulses have only two significant impurities, Ni and C, this ensuring a high degree of confidence in the results of the LINT analysis. The simulations for C suggest the need for an edge transport barrier and those for Ni provide information on the transport parameters for medium Z elements. No convection term is required except at the very edge of the plasma, where the choice was made to employ a convective edge barrier. The balance of the plasma particle inventory leads to a linear relationship between the outer diffusion coefficient used and the size of this barrier. Further understanding of the impurity behaviour in high performance discharges and of the technique itself will be gained by its wider application to different plasma machines.

APPENDIX - SOURCES OF ERROR IN THE TRANSPORT SIMULATIONS

A number of possible sources have been investigated for the discrepancies found between the simulations and the measured radiated powers and soft X-ray emission away from the plasma centre. These include additional radiation from the SOL, spatial asymmetries in the bulk radiation and errors in the sensitivity calibration of the VUV spectrometer, none of which can satisfactorily account for the discrepancies.

A1. Uncertainties in the T_e and n_e profiles.

Electron temperature and density profiles are input to the transport model and the sensitivity of the simulated results to possible errors in these profiles has been checked. The errors are expected to be largest towards the plasma edge and consequently the profiles have been varied outside a radius r/a of 0.7. Changing the T_e profile affected the ionization balance of the outer

stages and, consequently, the ratio of the NiXVIII to NiXVII emission. Increasing T_e, which improves the agreement of the radiated powers, although not the soft X-rays, reduced the simulated NiXVII ion density, thereby increasing the discrepancy in the NiXVIII line of sight measurements by more than 15%. The adjustment, ~30%, which would be required to the VUV spectrometer's relative sensitivity calibration to account for the NiXVIII discrepancy seems unacceptably large.

On the other hand, the worsening of the radiated power discrepancy when the temperature is reduced can be compensated by increasing the outer electron density and indeed, such profiles give the best overall fits. The results with modified T_e and n_e profiles are presented in table 4 for the corresponding simulation to that presented in table 3 for pulse 13738. It can be seen that the discrepancies in the radiated power and soft X-rays remain. The changes to the profiles were significant, a lowering of T_e by up to 300eV, which at the LCFS corresponded to a factor of 4 and up to a factor of 1.7 increase in n_e. The higher, outer n_e, which leads to a steepening of the n_e profile towards the plasma edge, is consistent with the changes required to give the best C simulations. However, these need the outer T_e to be increased rather than decreased, as gives the best Ni simulation.

A2. Uncertainties in the atomic data.

In the calculation of the total power radiated by an element using the ADAS data base, the power due to line radiation is separated from that due to recombination radiation and bremsstrahlung. These two components contribute roughly equally towards the soft X-rays, but the contribution of the line radiation to the total power is three times that of the recombination radiation and bremsstrahlung. The atomic data used to calculate the line radiation for the highest ionization stages, the lithium-like stage and above, are expected to be more reliable than those for the lower ionization stages, such as NiXV to NiXXV. The latter will dominate the total radiated power, the former contribute more to the soft X-rays. The discrepancy for the total radiated power might therefore indicate a limitation in the atomic data for the intermediate ionization stages of Ni.

A3. Soft X-ray emission profile reconstruction.

In all the simulations carried out, a discrepancy is found for the soft X-ray emission at radii away from the plasma centre. Crucially, the shape of the simulated and measured soft X-ray profiles always differ, the measured soft X-ray profile falling away more rapidly than can be explained by the simulation. Since agreement is found for the central soft X-ray emission, the atomic data appears to be satisfactory and the reconstruction of the soft X-ray emission profile is brought into question for these pulses.

ACKNOWLEDGEMENTS

We would like to thank Drs. K Guenther, L D Horton and A C Maas for useful discussions.

REFERENCES

Bartlett D V *et al*., 1987, Proc. 6th Int. Joint Workshop on ECE and ECRH, Oxford, JET Report JET-P(88)18

Behringer K H, 1987, Private communication

Bracco G *et al*., 1991, JET Report JET- R(91)02

Braithwaite G *et al*., 1989, Rev. Sci. Instrum., **60**, 2825

Denne-Hinnov B *et al*., 1993, Proc. 20th EPS Conf. on Controlled Fusion and Plasma Physics, Lisboa, **I**, 55

Edwards A W *et al*., 1986, Rev. Sci. Instrum., **57**, 2142

Erents S K *et al*., 1987, J. Nuclear Mater., **145-147**, 231

Fonck R J *et al*., 1982, Appl. Opt. **21**, 2115

Giannella R *et al*., 1994, Nuclear Fusion, **34**, 1185

Hawkes N C *et al*., 1992, Proc. 10th Int. Coll. UV and X-ray Spectroscopy of Astrophysical and Laboratory Plasmas, Berkeley, Ed: Silver E H and Kahn S M, C.U.P., Cambridge, 324

von Hellermann M G and Summers H P, 1993, Atomic and Plasma-Material Interaction Processes in Controlled Thermonuclear Fusion, Ed: Janev R K and Drawin H W, Elsevier, Amsterdam

Lauro-Taroni L *et al*., 1994, Proc. 21st EPS Conf. on Controlled Fusion and Plasma Physics, Montpellier, **I**, 102

Lawson K D *et al*. 1987, Task Agreement Note TAN(87) 1-3

Lipschultz B *et al*., 1984, Nuclear Fusion, **24**, 977

Mast K F *et al*., 1985, Rev. Sci. Instrum., **56**, 969

Morgan P D *et al*., 1985, Rev. Sci. Instrum., **56**, 862

Morgan P D and O'Rourke J J, 1987, Proc. 14th EPS Conf. on Controlled Fusion and Plasma Physics, Madrid, **III**, 1240

Schwob J L *et al*., 1987, Rev. Sci. Instrum., **58**, 1601

Taroni A and Tibone F, 1986, Proc. 13th EPS Conf. on Controlled Fusion and Plasma Heating, Schliersee, **I**, 160